Pramana – J. Phys. (2017) 89:81
https://doi.org/10.1007/s12043-017-1480-2

Three-dimensional coupled double-distribution-function lattice Boltzmann models for compressible Navier–Stokes equations

RUO-FAN QIU, YAN-CHENG YOU*, CHENG-XIANG ZHU, RONG-QIAN CHEN and JIAN-FENG ZHU

School of Aerospace Engineering, Xiamen University, Xiamen 361005, People's Republic of China
*Corresponding author. E-mail: yancheng.you@xmu.edu.cn

MS received 11 January 2017; revised 15 June 2017; accepted 23 June 2017; published online 14 November 2017

Abstract. Two three-dimensional (3D) lattice Boltzmann models in the framework of coupled double-distribution-function approach for compressible flows, in which specific-heat ratio and Prandtl number can be adjustable, are developed in this paper. The main differences between the two models are discrete equilibrium density and total energy distribution function. One is the D3Q25 model obtained from spherical function, and the other is the D3Q27 standard lattice model obtained from Hermite expansions of the corresponding continuous equilibrium distribution functions. The two models are tested by numerical simulations of some typical compressible flows, and their numerical stability and precision are also analysed. The results indicate that the two models are capable for supersonic flows, while the one from Hermite expansions is not suitable for compressible flows with shock waves.

Keywords. Lattice Boltzmann method; compressible flows; double distribution function; finite difference.

PACS Nos **47.11.–j; 51.10.+y; 05.20.Dd**

1. Introduction

The lattice Boltzmann method (LBM) [1–3] has become a prominent tool in computational fluid dynamic (CFD). Unlike the conventional numerical methods, which are based on discretization of macroscopic governing equations, and unlike the molecular dynamics method, which is based on molecular representation with complicated molecule collision rules, the LBM is based on microscopic models and mesoscopic kinetic equations for particle distribution functions. It simulates fluid flows by tracking the evolutions of the distribution functions and then accumulates the distributions to obtain macroscopic averaged properties. As a mesoscopic numerical method based on the kinetic theory, LBM can describe complex flows from an intuitive view of particle distribution. Its advantages include high efficiency in parallel computing, complex boundary conditions can be easily formulated in terms of elementary mechanics rules, and simple programming [4,5]. It has been applied to various fluid applications successfully [6–13].

The basic idea of LBM is to solve discrete Boltzmann Bhatnagar–Gross–Krook (BGK) equation, in which the key issue is the distribution function. The distribution function is the discrete velocity Boltzmann equation (DVBE)-based method. Once the DVBE model is determined, the fluid flows can be simulated by solving the Boltzmann BGK equation directly. The number of DVBE and expression of distribution functions are determined according to specific physical problems. For instance, the distribution function should satisfy constraints with five equations in order for BGK equation to recover the conventional Euler equation, while it is seven equations for Navier–Stokes equation. This leads to more complex DVBE model for the latter. The widely used two-dimensional nine-velocity (D2Q9) DVBE model [1], which is also called standard lattice model, is usually applied for incompressible isothermal fluid flow. When it comes to thermal or compressible problem, the standard D2Q9 DVBE model is not enough to satisfy constraints. Then, more complex DVBE models or additional treatments are needed. For the sake of clarity, we focus on compressible fluid flows.

The main approaches for constructing compressible fluid flow fall into two classes: the multispeed approach [14–20] and the double-distribution-function (DDF) approach [21–25]. The multispeed approach is a straightforward extension of the incompressible isothermal LBM. In this approach higher-order velocity moments of the density distribution function are used to

describe more equations. The first multispeed approach was devised by Alexander *et al* as a third-order D2Q13 model [14]. Yan *et al* proposed a D2Q17 model with two rest energy levels, which can recover the Euler equation [15]. Kataoka and Tsutahara proposed a D2Q16 model for compressible Navier–Stokes equations with a flexible specific-heat ratio [16]. Qu *et al* proposed a D2Q13 model for inviscid compressible flows with adjustable specific-heat ratio, in which the conventional Maxwellian distribution function is replaced by a circular function. This model has the ability for the simulation of compressible flows at high Mach number [17]. Watari proposed a 2D model with 65 discrete velocities for Navier–Stokes that allow arbitrary values to be set for the specific heat ratio [18]. Recently, Xu and his coworkers have done a lot of work in multispeed approach for compressible flows: Gan *et al* improved Watari's model [18] for high Mach number [26] and flexible Prandtl (Pr) number [27]. Chen *et al* developed Kataoka and Tsutahara's model [16] by introducing artificial viscosity [28] and using multiple-relaxation-time (MRT) scheme [29], respectively; Gan *et al* proposed a D2Q16 model for compressible Navier–Stokes equations with adjustable specific heat ratio [19]. Following Gan *et al*'s idea, Xu *et al* proposed a D2Q24 MRT model for combustion [20]. In multispeed approach, in order to satisfy 2D compressible Navier–Stokes equations with a flexible specific-heat ratio and Pr number, the lattice Boltzmann (LB) model will become very complex, not to mention 3D cases.

Fortunately, these terms can be easily considered in the DDF approach, which makes LB equation and DVBE quite clear and simple. The DDF approach utilizes two different distribution functions, one for the flow field and the other for the temperature field. The first DDF model was devised by He *et al* [21]. This model has attracted much attention since its emergence because of its excellent numerical stability and adjustability of the Pr number. However, this model includes complicated gradient terms involving temporal and spatial derivatives of the macroscopic flow variables, which may introduce some additional errors and harm the numerical stability. Inspired by He *et al*'s idea, Guo *et al* proposed another version by introducing a total energy distribution function to replace the internal energy distribution function [22]. This is a decoupling model that the temperature field does not affect the flow field. Following Guo *et al*'s treatment, Li *et al* proposed a coupled finite-difference (FD) DDF model for 2D compressible Navier–Stokes equations with a flexible specific-heat ratio and Pr number [23]. They also introduce Qu *et al*'s [17] DVBE into the model to achieve high Mach number. Wang *et al* also developed a DDF LB model for viscous compressible flows with flexible specific-heat ratio and Prandtl number with a different total energy distribution function [24]. Li *et al* proposed a coupled DDF LB model on standard D2Q9 lattice model, which can deal with flows at low Mach number with streaming-collision process [25]. The distribution functions are obtained from the Hermite expansions of the corresponding continuous equilibrium distribution functions.

Although LBM has been well developed in compressible flows, there is a very few 3D compressible LB modes, especially for compressible Navier–Stokes equations with a flexible specific-heat ratio and Pr number. Kataoka and Tsutahara presented a D3Q15 model for compressible Euler equations [30]. This model is only for subsonic flows. Chen *et al* improved Kataoka and Tsutahara's [30] model for high-speed flow [31]. Watari and Tsutahara proposed a D3Q73 model for Euler equations, which can achieve Mach number 1.7 [32]. Li *et al* developed Qu *et al*'s [17] D2Q13 model to D3Q25 model for compressible Euler equations [33]. He *et al* proposed a 3D DDF LB model for compressible Navier–Stokes equations [34]. It can be seen that most 3D compressible LB models are for Euler equations. If the treatments of the existing 2D model for Navier–Stokes equations are complicated, their 3D models will become much more complex.

In this paper, two 3D DDF LB models for compressible Navier–Stokes equations with flexible specific-heat ratio and Pr number are developed. They can be viewed as extended work of Li *et al* in ref. [23] and ref. [25]. This work presents alternative 3D LB models for compressible flows, and shows the convenience and simplicity of DDF approach. The rest of the paper is organized as follows. In §2, the basic method for constructing DDF LB model is described, and two 3D models are given. In §3, numerical simulations are carried out for some typical compressible flows to test the models. Finally, conclusions are drawn in §4.

2. Three-dimensional compressible coupled double-distribution-function model

2.1 *Coupled double-distribution-function approach for Navier–Stokes equations*

The DDF LB approach is also called the two-relaxation-time kinetic model [23–25]. The kinetic equations from the Boltzmann equation with the BGK approximation for the two-relaxation-time kinetic model can be written as follows:

$$\frac{\partial f_\alpha}{\partial t} + (\mathbf{e}_\alpha \cdot \nabla) f_\alpha = -\frac{1}{\tau_f}(f_\alpha - f_\alpha^{\mathrm{eq}}), \tag{1}$$

$$\frac{\partial h_\alpha}{\partial t} + (\mathbf{e}_\alpha \cdot \nabla)\, h_\alpha = -\frac{1}{\tau_h}(h_\alpha - h_\alpha^{\mathrm{eq}}) + \frac{1}{\tau_{hf}}\,(\mathbf{e}_\alpha \cdot \mathbf{u})\,(f_\alpha - f_\alpha^{\mathrm{eq}}), \quad (2)$$

where f_α is the density distribution function and h_α is the total energy distribution function, f_α^{eq} and h_α^{eq} are the corresponding equilibrium distribution functions, $\mathbf{e}_\alpha$ is the discrete particle velocity in α direction, $\mathbf{u}$ is the macroscopic velocity, τ_f and τ_h are density and energy relaxation times, and τ_{hf} is defined as $\tau_{hf} = \tau_h\tau_f/(\tau_f - \tau_h)$. τ_f can be determined by the equation $\tau_f = \mu/p$, where μ is the dynamic viscosity and $p = \rho RT$ is the pressure, in which R is the specific gas constant and T is the temperature. The Pr number of the system can be made arbitrary by adjusting the two relaxation times as $\mathrm{Pr} = \tau_f/\tau_h$.

The equilibrium density distribution function should satisfy the following velocity moment condition to recover the compressible Navier–Stokes equations:

$$\sum_\alpha f_\alpha^{\mathrm{eq}} = \rho, \quad (3a)$$

$$\sum_\alpha f_\alpha^{\mathrm{eq}} e_{\alpha i} = \rho u_i, \quad (3b)$$

$$\sum_\alpha f_\alpha^{\mathrm{eq}} e_{\alpha i} e_{\alpha j} = \rho u_i u_j + p\delta_{ij}, \quad (3c)$$

$$\sum_\alpha f_\alpha^{\mathrm{eq}} e_{\alpha i} e_{\alpha j} e_{\alpha k} = \rho u_i u_j u_k + p(u_k\delta_{ij} + u_j\delta_{ik} + u_i\delta_{jk}), \quad (3d)$$

where ρ is the density. The subscripts i, j and k indicate the x, y or z component. δ_{ij}, δ_{ik} and δ_{jk} are the Kronecker delta functions.

The equilibrium total energy distribution function should satisfy the following velocity moment condition:

$$\sum_\alpha h_\alpha^{\mathrm{eq}} = \rho E, \quad (4a)$$

$$\sum_\alpha e_{\alpha i} h_\alpha^{\mathrm{eq}} = (\rho E + p)\, u_i, \quad (4b)$$

$$\sum_\alpha e_{\alpha i} e_{\alpha j} h_\alpha^{\mathrm{eq}} = (\rho E + 2p)\, u_i u_i + p(E + RT)\,\delta_{ij}, \quad (4c)$$

where $E = bRT/2 + u^2/2$ is the total energy, b is a constant, which is related to the specific-heat ratio γ by $\gamma = (b+2)/b$.

So far, the framework of coupled DDF LB approach for compressible Navier–Stokes equations with flexible specific-heat ratio and Pr number is given. Once the DVBE model, in which the density distribution function f_α^{eq} and the total energy distribution function h_α^{eq} satisfy eqs (3) and (4) respectively, is determined for 3D case, the coupled DDF LB model is established.

2.2 *Discrete velocity Boltzmann equation model*

In the LB community, the equilibrium distribution function can be determined by several methods. The widely used method is based on the Maxwellian equilibrium distribution function, which includes the Taylor expansion approach [35] and the Hermite expansion approach [36]. The former is limited to low- and moderate-Mach-number flows, which mainly results from the Taylor expansion in terms of the Mach number and too many free parameters [16,23]. The latter allows for simulating high-Mach-number flows. There are also some methods that use another function, which satisfies the needed statistical relations (as eqs (3) and (4)) and is employed to replace the Maxwellian function as the continuous equilibrium distribution function to simulate high-Mach-number flows [17,37].

In this subsection, we show two DVBE models for 3D DDF LB model, in which equilibrium distribution functions are obtained from spherical function and Maxwellian equilibrium distribution function by Hermite expansion, respectively.

2.2.1 *Spherical function-based model.*

Qu *et al* proposed the method to construct equilibrium distribution function by circular function [17]. Li *et al* introduced this 2D model into the coupled DDF model for the equilibrium density distribution function [23], while a simple and general model is adopted for the equilibrium total energy distribution function. Here we extended this D2Q13 DVBE model for the 3D case. Fortunately, Li *et al* have proposed a 3D model based on spherical function [33], which follows Qu *et al*'s idea about circular function in the 2D case. We adopted this D3Q25 DVBE model (figure 1) for the equilibrium density distribution function,

$$e_\alpha = \begin{cases} (0,0,0), & \alpha = 0, \\ (1,0,0)_{\mathrm{FS}}\tilde{c}, & \alpha = 1,2,\ldots,6, \\ (1,1,0)_{\mathrm{FS}}\tilde{c}, & \alpha = 7,8,\ldots,18, \\ (2,0,0)_{\mathrm{FS}}\tilde{c}, & \alpha = 19,20,\ldots,24, \end{cases} \quad (5)$$

where $\tilde{c} = \sqrt{3RT_c}$ is the characteristic speed of the lattice fluid, in which T_c is the characteristic temperature, and the subscript 'FS' denotes a fully symmetric set of points.

The 3D equilibrium density distribution function based on spherical function is given by

$$f_0^{\mathrm{eq}} = \frac{1}{60}\rho(60 - 75\bar{r}^2 - 75\bar{u}^2 - 75\bar{v}^2 - 75\bar{w}^2 + 21\bar{r}^4 + 15\bar{u}^4 + 15\bar{v}^4 + 15\bar{w}^4 + 70\bar{u}^2\bar{r}$$

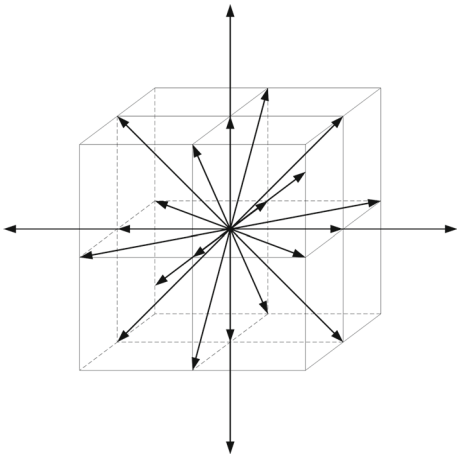

Figure 1. Discrete velocities of the D3Q25 model.

$$+70\bar{v}^2\bar{r}+70\bar{w}^2\bar{r}+60\bar{u}^2\bar{v}^2+60\bar{u}^2\bar{w}^2 +60\bar{v}^2\bar{w}^2), \tag{6a}$$

$$f_1^{\mathrm{eq}}=-\frac{1}{90}\rho(15\bar{u}^4+15\bar{u}^3-60\bar{u} +45\bar{u}\bar{r}^2+45\bar{u}\bar{v}^2+45\bar{u}\bar{w}^2 +45\bar{u}^2\bar{v}^2+45\bar{u}^2\bar{w}^2+60\bar{u}^2\bar{r}^2 +15\bar{v}^2\bar{r}^2+15\bar{w}^2\bar{r}^2-60\bar{u}^2 +9\bar{r}^4-20\bar{r}^2), \tag{6b}$$

$$f_7^{\mathrm{eq}}=\frac{1}{60}\rho(15\bar{u}^2\bar{v}^2+15\bar{u}^2\bar{v}+15\bar{u}\bar{v}^2 +15\bar{u}\bar{v}+5\bar{u}^2\bar{r}^2+5\bar{v}^2\bar{r}^2 +5\bar{u}\bar{r}^2+5\bar{v}\bar{r}^2+\bar{r}^4), \tag{6c}$$

$$f_{19}^{\mathrm{eq}}=\frac{1}{360}\rho(15\bar{u}^4+30\bar{u}^3+30\bar{u}^2\bar{r}^2+30\bar{u}\bar{r}^2 -15\bar{u}^2-30\bar{u}-5\bar{r}^2+3\bar{r}^4), \tag{6d}$$

and others are

$$\begin{aligned}
f_2^{\mathrm{eq}}(\bar{u},\bar{v},\bar{w})&=f_1^{\mathrm{eq}}(-\bar{u},\bar{v},\bar{w}),\\
f_3^{\mathrm{eq}}(\bar{u},\bar{v},\bar{w})&=f_1^{\mathrm{eq}}(\bar{v},\bar{u},\bar{w}),\\
f_4^{\mathrm{eq}}(\bar{u},\bar{v},\bar{w})&=f_1^{\mathrm{eq}}(-\bar{v},\bar{u},\bar{w}),\\
f_5^{\mathrm{eq}}(\bar{u},\bar{v},\bar{w})&=f_1^{\mathrm{eq}}(\bar{w},\bar{v},\bar{u}),\\
f_6^{\mathrm{eq}}(\bar{u},\bar{v},\bar{w})&=f_1^{\mathrm{eq}}(-\bar{w},\bar{v},\bar{u}),\\
f_8^{\mathrm{eq}}(\bar{u},\bar{v},\bar{w})&=f_7^{\mathrm{eq}}(-\bar{u},-\bar{v},\bar{w}),\\
f_9^{\mathrm{eq}}(\bar{u},\bar{v},\bar{w})&=f_7^{\mathrm{eq}}(\bar{u},-\bar{v},\bar{w}),\\
f_{10}^{\mathrm{eq}}(\bar{u},\bar{v},\bar{w})&=f_7^{\mathrm{eq}}(-\bar{u},\bar{v},\bar{w}),\\
f_{11}^{\mathrm{eq}}(\bar{u},\bar{v},\bar{w})&=f_7^{\mathrm{eq}}(\bar{u},\bar{w},\bar{v}),\\
f_{12}^{\mathrm{eq}}(\bar{u},\bar{v},\bar{w})&=f_7^{\mathrm{eq}}(-\bar{u},-\bar{w},\bar{v}),\\
f_{13}^{\mathrm{eq}}(\bar{u},\bar{v},\bar{w})&=f_7^{\mathrm{eq}}(\bar{u},-\bar{w},\bar{v}),\\
f_{14}^{\mathrm{eq}}(\bar{u},\bar{v},\bar{w})&=f_7^{\mathrm{eq}}(-\bar{u},\bar{w},\bar{v}),\\
f_{15}^{\mathrm{eq}}(\bar{u},\bar{v},\bar{w})&=f_7^{\mathrm{eq}}(\bar{v},\bar{w},\bar{u}),
\end{aligned} \tag{6e}$$

$$\begin{aligned}
f_{16}^{\mathrm{eq}}(\bar{u},\bar{v},\bar{w})&=f_7^{\mathrm{eq}}(-\bar{v},-\bar{w},\bar{u}),\\
f_{17}^{\mathrm{eq}}(\bar{u},\bar{v},\bar{w})&=f_7^{\mathrm{eq}}(\bar{v},-\bar{w},\bar{u}),\\
f_{18}^{\mathrm{eq}}(\bar{u},\bar{v},\bar{w})&=f_7^{\mathrm{eq}}(-\bar{v},\bar{w},\bar{u}),
\end{aligned} \tag{6f}$$

$$\begin{aligned}
f_{20}^{\mathrm{eq}}(\bar{u},\bar{v},\bar{w})&=f_{19}^{\mathrm{eq}}(-\bar{u},\bar{v},\bar{w}),\\
f_{21}^{\mathrm{eq}}(\bar{u},\bar{v},\bar{w})&=f_{19}^{\mathrm{eq}}(\bar{v},\bar{u},\bar{w}),\\
f_{22}^{\mathrm{eq}}(\bar{u},\bar{v},\bar{w})&=f_{19}^{\mathrm{eq}}(-\bar{v},\bar{u},\bar{w}),\\
f_{23}^{\mathrm{eq}}(\bar{u},\bar{v},\bar{w})&=f_{19}^{\mathrm{eq}}(\bar{w},\bar{v},\bar{u}),\\
f_{24}^{\mathrm{eq}}(\bar{u},\bar{v},\bar{w})&=f_{19}^{\mathrm{eq}}(-\bar{w},\bar{v},\bar{u}),
\end{aligned} \tag{6g}$$

where $\bar{u}=u_x/\tilde{c}$, $\bar{v}=u_y/\tilde{c}$, $\bar{w}=u_z/\tilde{c}$ and $\bar{r}=\sqrt{T/T_c}$. $f_3^{\mathrm{eq}}(\bar{u},\bar{v},\bar{w})=f_1^{\mathrm{eq}}(\bar{v},\bar{u},\bar{w})$ means $f_3^{\mathrm{eq}}(\bar{u},\bar{v},\bar{w})$ is calculated with the same form of $f_1^{\mathrm{eq}}(\bar{v},\bar{u},\bar{w})$, and the locations of the parameters in $f_1^{\mathrm{eq}}(\bar{v},\bar{u},\bar{w})$ are permuted.

Besides, the equilibrium total energy distribution function of the model has the relationship with corresponding equilibrium density distribution function as:

$$h_\alpha^{\mathrm{eq}}=[E+(e_\alpha-\mathbf{u})\cdot\mathbf{u}]f_\alpha^{\mathrm{eq}}+\varpi_\alpha\frac{p}{\tilde{c}^2}RT, \tag{7}$$

where ϖ_α should satisfy the constraints as follows [23]:

$$\sum_\alpha\varpi_\alpha\frac{p}{\tilde{c}}RT=0, \tag{8a}$$

$$\sum_\alpha e_{\alpha i}\varpi_\alpha\frac{p}{\tilde{c}^2}RT=0, \tag{8b}$$

$$\sum_\alpha e_{\alpha i}e_{\alpha j}\varpi_\alpha\frac{p}{\tilde{c}^2}RT=pRT\delta_{ij}. \tag{8c}$$

The above equations give constraints for ϖ_0, $\varpi_{1,2,\ldots,6}$, $\varpi_{7,8,\ldots,18}$ and $\varpi_{19,20,\ldots,24}$ as follows:

$$\varpi_0+6\varpi_{1,2,\ldots,6}+12\varpi_{7,8,\ldots,18}+6\varpi_{19,20,\ldots,24}=0, \tag{9a}$$

$$\varpi_{1,2,\ldots,6}+4\varpi_{7,8,\ldots,18}+4\varpi_{19,20,\ldots,24}=1/2, \tag{9b}$$

which are obviously not enough for determining these parameters. We have to choose some of them artificially. In this paper, we adopted $\varpi_0=0$, $\varpi_{1,2,\ldots,6}=-5.0/14$, $\varpi_{7,8,\ldots,18}=1.0/7$ and $\varpi_{19,20,\ldots,24}=1.0/14$. It should be noticed that selection of these parameters will influence the numerical stability of the model. Besides, as this DDF model uses different kinds of equilibrium distribution functions for density and total energy, the consistency of the model is not very good, which has some impact on numerical stability. Thus, although Li *et al* [23] have shown good numerical stability for the 2D DDF model, the performance of the present 3D model should be further examined.

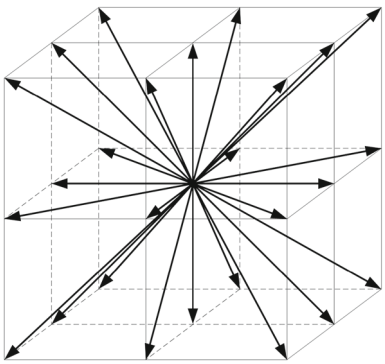

Figure 2. Discrete velocities of the D3Q27 model.

2.2.2 *Hermite expansions-based model.* Shan *et al* presented the determination method of equilibrium distribution function by the Hermite expansion approach [36]. In the Hermite expansion approach, the equilibrium distribution function can be determined by projecting the Maxwellian function onto the tensor Hermite polynomial basis in terms of the particle velocity and up to a certain order. As pointed out by Shan *et al*, the Hermite expansion approach allows for simulations of high Mach number flows. Li *et al* introduced this method into the DDF LB approach and formulated a thermal model on standard lattices with D2Q9 model [25]. Following this idea, we adopted D3Q27 standard DVBE model (figure 2) for the 3D coupled DDF compressible model,

$$e_\alpha = \begin{cases} (0,0,0), & \alpha = 0, \\ (1,0,0)_{\mathrm{FS}}\tilde{c}, & \alpha = 1,2,\ldots,6, \\ (1,1,0)_{\mathrm{FS}}\tilde{c}, & \alpha = 7,8,\ldots,18, \\ (\pm1,\pm1,\pm1)\,\tilde{c}, & \alpha = 19,20,\ldots,26, \end{cases} \tag{10}$$

where $\tilde{c} = \sqrt{3RT_c}$.

In order to satisfy eqs (3) and (4), third-order expansion and second-order Hermite expansions are used for f^{eq} and h^{eq}, respectively [25,36]. Therefore, they can be written as follows:

$$\begin{aligned} f_\alpha^{\mathrm{eq}} = \varpi_\alpha \rho \Big\{ & 1 + \widehat{e}_\alpha \cdot \widehat{\mathbf{u}} + \tfrac{1}{2}\Big[\left(\widehat{e}_\alpha \cdot \widehat{\mathbf{u}}\right)^2 - \widehat{u}^2 \\ & + (\theta - 1)\left(\widehat{e}_\alpha^2 - D\right)\Big] + \tfrac{\widehat{e}_\alpha \cdot \widehat{\mathbf{u}}}{6}\Big[\left(\widehat{e}_\alpha \cdot \widehat{\mathbf{u}}\right)^2 \\ & - 3\widehat{u}^2 + 3(\theta - 1)\left(\widehat{e}_\alpha^2 - D - 2\right)\Big]\Big\} \end{aligned} \tag{11a}$$

$$\begin{aligned} h_\alpha^{\mathrm{eq}} = & E f_\alpha^{\mathrm{eq}} \\ & + \varpi_\alpha p \left[\widehat{e}_\alpha \cdot \widehat{\mathbf{u}} + \left(\widehat{e}_\alpha \cdot \widehat{\mathbf{u}}\right)^2 - \widehat{u}^2 + \frac{\theta}{2}(\widehat{e}_\alpha^2 - D)\right], \end{aligned} \tag{11b}$$

where $\widehat{e}_\alpha = e_\alpha/\sqrt{RT_c}$, $\widehat{\mathbf{u}} = \mathbf{u}/\sqrt{RT_c}$, $\theta = T/T_c$ and D is the spatial dimension.

Since this D3Q27 DVBE model is on standard lattices, the simple and effective streaming-collision process can be implemented, which means the basic advantages of the standard LBM are retained. In this paper, for convenience and stability, we adopted FD approach for simulation like the D3Q25 model above.

2.2.3 *Analysis of the two DVBE models.* Here, we make a preliminary discussion about the two DVBE models. In the spherical function-based model, a complete third-order polynomial with 19 terms for the 3D case is needed for f^{eq} to satisfy eq. (3). However, it would be difficult to form a symmetric lattice velocity model with 19 points. Then additional 6 fourth-order terms are used. And h^{eq} is given by the relationship with the corresponding f^{eq}. In the Hermite expansions-based model, f^{eq} and h^{eq} are formulated through third-order expansion and second-order Hermite expansion, respectively. From this point of view, the D3Q25 spherical function-based model has higher order than the D3Q27 Hermite expansion-based model in equilibrium distribution function.

On the other hand, the stability strongly depends on the positivity of the equilibrium function. The positivity ranges of f^{eq} and h^{eq} for the two models are studied through one-dimensional analysis [38], in which the Mach number is defined as $\mathrm{Ma} = u/\sqrt{RT_c}$ and $b = 5$. Figure 3 gives the positivity region of the equilibrium functions. The shaded area is where all f^{eq} or h^{eq} are positive. For the spherical function-based model, f^{eq} may be negative when Mach number is smaller than 2 at low temperature, while f^{eq} is positive when Mach number is larger than 2. h^{eq} at high Mach number are positive only when the temperature is also high. On the contrary, f^{eq} and h^{eq} are positive at low Mach number and temperature in the Hermite expansion-based model. Thus, the spherical function-based model is more stable at high Mach number, while the Hermite expansion-based model is the opposite.

The two DVBE models are based on different approaches, which results in their different numerical features. Thus, we shall compare their performance using several numerical tests below.

3. Numerical tests

In this section, the two 3D coupled DDF models are tested by several numerical cases with compressible flows ranging from 1D to 3D. For convenience, the spherical function-based model and the Hermite expansion-based model are called Model I and Model II, respectively. To solve eqs (1) and (2) numerically, the first-order implicit-explicit (IMEX) Runge–Kutta

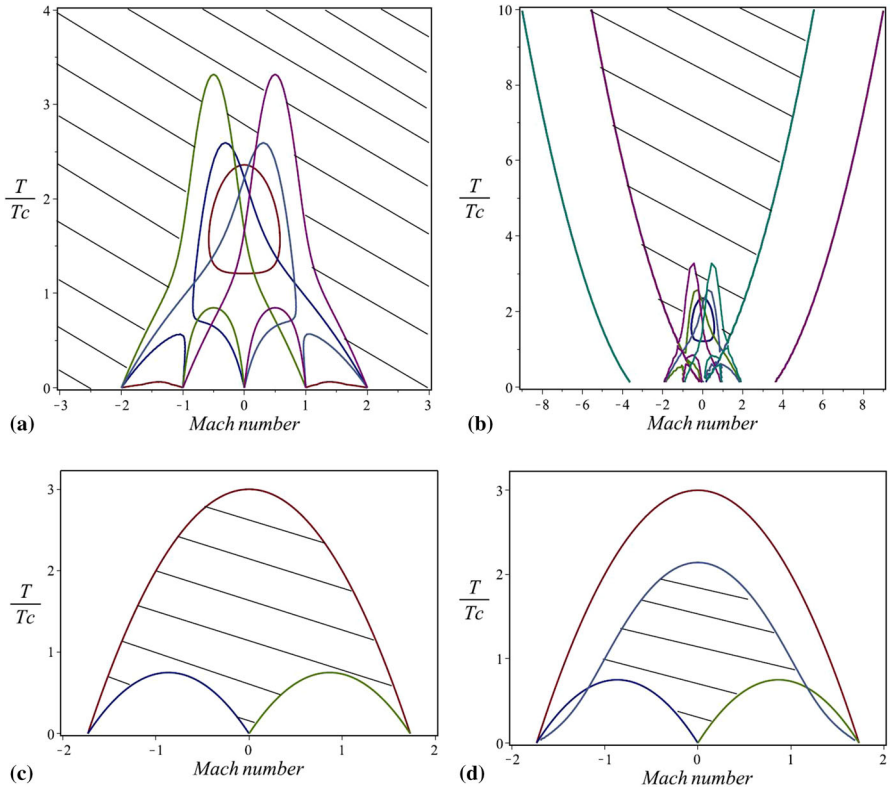

Figure 3. Positivity region (shaded) of all the f^{eq} and h^{eq} in the two models: (**a**) f^{eq} of the spherical function-based model, (**b**) h^{eq} of the spherical function-based model, (**c**) f^{eq} of the Hermite expansion-based model, (**d**) h^{eq} of the Hermite expansion-based model.

scheme [39,40] is employed for the time discretization and the non-free-parameter dissipation (NND) scheme [41], which is a total variation diminishing (TVD) scheme, is applied for the space discretization. The reference density ρ_0, the reference temperature T_0, the reference length L_0 and the time spacing Δt are used in the simulations, and the reference velocity and the reference pressure are defined as $u_0 = \sqrt{RT_0}$, $p_0 = \rho_0 RT_0$. Here, $\rho_0 = 1.165\ \mathrm{kg/m^3}$, $R = 287\ \mathrm{J/(kg\ K)}$, $T_0 = 303\,\mathrm{K}$, $\mu = 1.86 \times 10^{-5}\ \mathrm{kg/(m\ s)}$, $\tau_0 = \mu/p_0$. The specific-heat ratio is set to be 1.4 with $b = 5$ and the Prandtl number is set to be 0.71. The relaxation times are $\tau_f = 1.84 \times 10^{-10}$ and $\tau_h = 2.59 \times 10^{-10}$.

3.1 1*D Riemann problems*

The 1D Riemann problem is a typical case for testing numerical methods in the simulation of compressible flows. We conducted the Sod shock tube with initial condition as follows:

$$(\rho/\rho_0, u_x/u_0, p/p_0) = (1.0, 0, 1.0)\,, \quad 0 < x/L_0 \le \frac{1}{2},$$

$$(\rho/\rho_0, u_x/u_0, p/p_0) = (0.125, 0, 0.1)\,, \frac{1}{2} < x/L_0 < 1.$$

The $N_x \times N_y \times N_z = 400 \times 5 \times 5$ lattices are used, where N_x, N_y and N_z are lattice numbers along the x, y and z directions, respectively. In the x direction, $f_\alpha = f_\alpha^{\mathrm{eq}}$ is set and the periodic boundary conditions are imposed in the y and z directions. The characteristic time of the system is defined as $t_0 = L_0/u_0$ and $L_0 = 2m$. In the simulations, $T_c = 4/3T_0$ is set for Model I and $T_c = 2T_0$ is set for Model II, and $\Delta t = 30000\tau_0$. Simulation results by Models I and II of the Sod shock tube at $t = 0.1644t_0$ are given in figure 4. Generally speaking, the results by the two models agree well with the analytical solutions. Both the models have some numerical fluctuations between $x/L_0 = 0.6$ and $x/L_0 = 0.8$, especially for the temperature distribution. This may be caused by the time discretization that just first-order IMEX Runge–Kutta scheme we used. Besides, a little deviation appears at about $x/L_0 = 0.5$ for Model II. The magnified results between $x/L_0 = 0.46$ and $x/L_0 = 0.54$ are shown in figure 5. Although the same FD schemes are used by the two models, results by Model II disagrees with analytical solutions at about $x/L_0 = 0.5$, while Model I still performs well. That is,

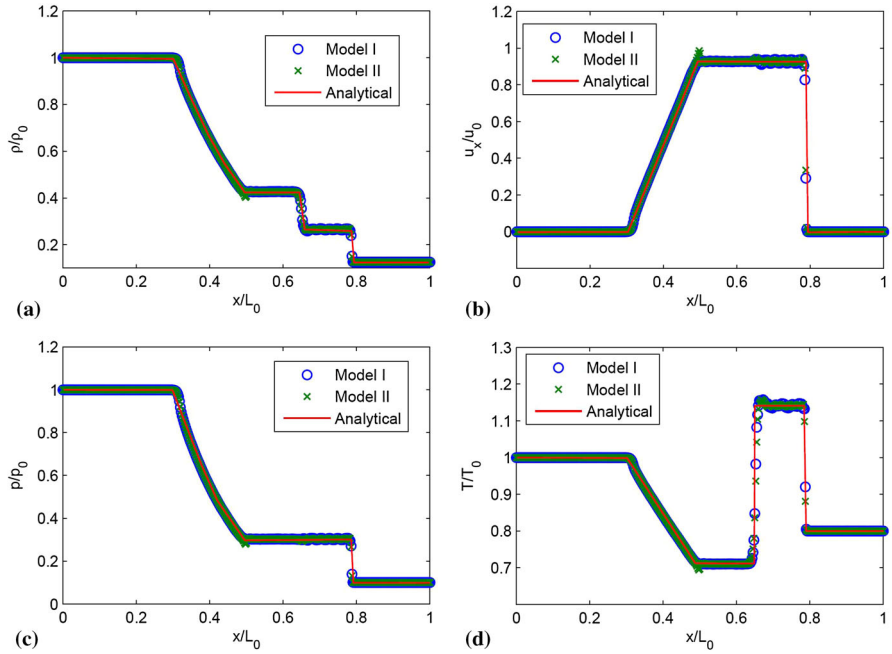

Figure 4. Simulation results by Models I and II of the Sod shock tube for (**a**) density, (**b**) velocity, (**c**) pressure, (**d**) temperature.

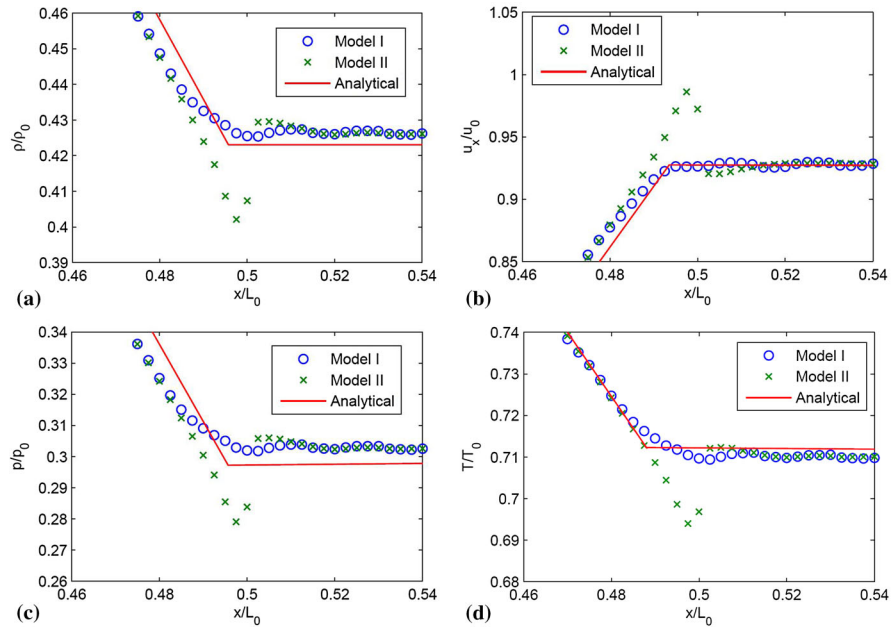

Figure 5. Comparisons of discontinuity between Models I and II in Sod shock tube simulation for (**a**) density, (**b**) velocity, (**c**) pressure, (**d**) temperature.

Model II is not very good at simulating compressible flows with discontinuity.

3.2 *2D Couette flow*

The Couette flow is a classical heat-transfer problem which can provide a good test of numerical model to describe viscous heat dissipation. Consider a viscous fluid flow between two infinite parallel flat plates, separated by a distance H. The top plate at temperature T_1 moves at speed U, and the bottom plate at temperature T_0 is stationary. In a steady state, the temperature profiles satisfy the following relation when the variation of the viscosity and thermal conductivity is neglected:

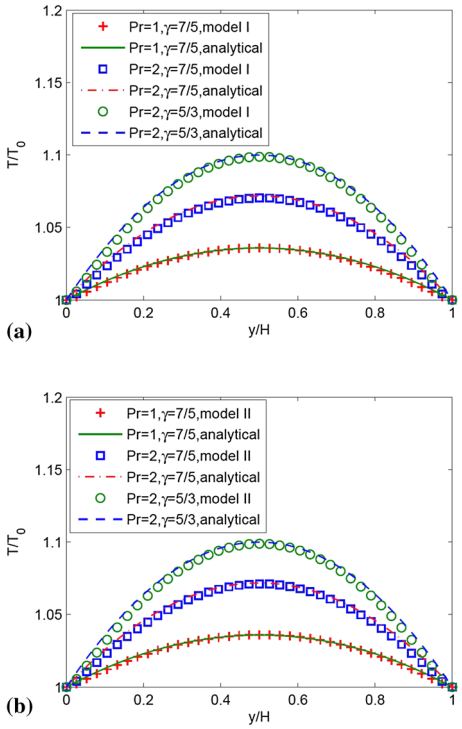

Figure 6. Dimensionless temperature profiles in steady Couette flow at $U = u_0$ for different Pr and γ by (**a**) Model I and (**b**) Model II.

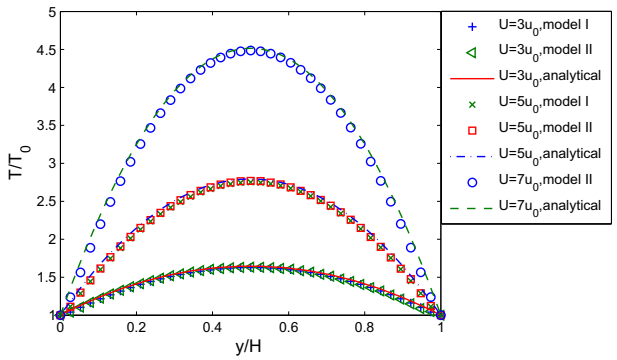

Figure 7. Dimensionless temperature profiles in steady Couette flow at different U by Models I and II.

$$T_1 = T_0 : T - T_0 = \Pr \frac{U^2}{2c_p} \frac{y}{H} \left(1 - \frac{y}{H}\right), \tag{12}$$

where y is the distance from the bottom boundary. $N_x \times N_y \times N_z = 40 \times 40 \times 5$ lattices are adopted. The periodic boundary condition is applied to the inlet and outlet in x direction, the nonequilibrium extrapolation method [42] is applied to the two plates in y direction, and the periodic boundary condition is also implemented in z direction. In the simulations, $T_c = 4/3T_0$ is set for Model I and $T_c = 2/3T_0$ is set for Model II, and other parameters are $L_0 = 2.7 \times 10^{-6}$ m, $\Delta t = 0.1\tau_0$. The dimensionless temperature profiles in steady Couette flow at $U = u_0$ for different Pr and γ by the two models are given in figure 6. The results by the two models agree well with the analytical results. The Mach number in this case is 0.85. We also tested their performances for high Mach numbers. Figure 7 shows dimensionless temperature profiles in steady Couette flow at $U = 3u_0$, $U = 5u_0$ and $U = 7u_0$, in which Mach numbers are 2.54, 4.23 and 5.92 respectively, by the two models. The characteristic temperature is $T_c = 40/3T_0$ for the two models in this case. They both agree well with the analytical results at $U = 3u_0$ and $U = 5u_0$. However, at $U = 7u_0$, Model I becomes unstable, while model still works well. We found that selection of ϖ_α influences stability of Model I here. At present, the two models are both suitable for high Mach number flows without shock wave, and the numerical stability of Model II is better than Model I. Besides, the FD schemes also have influence on their numerical stability. One can choose higher order or more appropriate FD schemes for better numerical stability.

3.3 *2D regular shock reflection*

A steady 2D compressible flow, a regular shock reflection on a wall, is considered in this test. This problem involves three flow regions separated by an oblique shock and its reflection from a wall. The incoming shock wave of Mach number 2.9 has an incident angle to the wall. The Dirichlet conditions

$$(\rho/\rho_0, u_x/u_0, u_y/u_0, u_z/u_0, p/p_0)|_{\text{Left}} = (1.0, 2.9, 0, 0, 1.0/1.4),$$
$$(\rho/\rho_0, u_x/u_0, u_y/u_0, u_z/u_0, p/p_0)|_{\text{Top}} = (1.69997, 2.61934, -0.50633, 0, 1.52819).$$

are imposed on the left and top boundaries, respectively. The bottom boundary is a reflecting surface. The right boundary is the supersonic outflow where the zeroth-order extrapolation is used. The periodic boundary condition is applied in the z direction. $N_x \times N_y \times N_z = 150 \times 50 \times 5$ lattices are used. The two models are also tested in this case. Unfortunately, Model II failed, while Model I performs well. That is, Model II is not suitable for dealing with compressible flows with shock wave. The exact reason for the failure of Model II is still unknown. However, according to our preliminary discussion about the two models above, the equilibrium distribution function in Model I has higher order than Model II, and this may be a possible reason.

Figure 8 gives numerical results of the regular shock reflection problem by Model I. In the simulations,

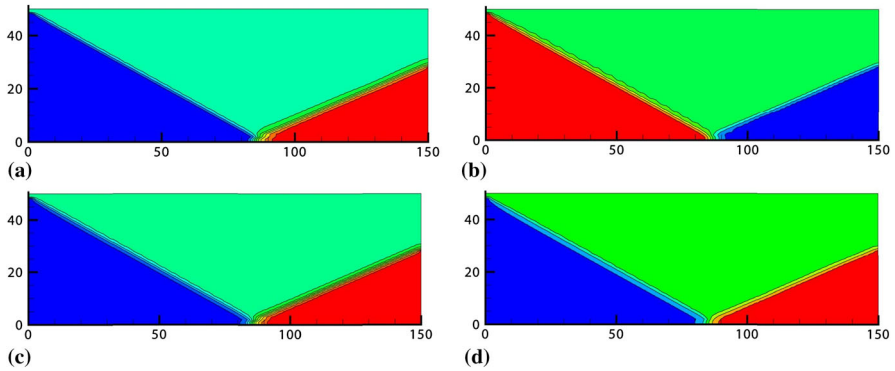

Figure 8. Numerical results of regular shock reflection problem by Model I for (**a**) density, (**b**) velocity in x direction, (**c**) pressure, (**d**) temperature.

$T_c = 2T_0$ and $\Delta t = 20000\tau_0$. The density, velocity, pressure and temperature contours in which the shock reflection are well captured, are shown.

3.4 *3D explosion in a box*

The case of 3D explosion in a box [43], in which a spherical shock wave expands in an enclosed box, is tested by the two models. It is an unsteady 3D compressible flow and the reflected shocks interact in a complex manner. The computational domain is $[0, 1.0] \times [0, 1.0] \times [0, 1.0]$. At the initial time, the velocity is zero; $\rho/\rho_0 = 5.0$ and $p/p_0 = 5.0$ are set in a sphere with radius 0.3, whose centre is at (0.4, 0.4, 0.4), and $\rho/\rho_0 = 1.0$ and $p/p_0 = 1.0$ are set for others.

In the simulations, a $N_x \times N_y \times N_z = 100 \times 100 \times 100$ mesh is used. The rest of the parameters are set to be $T_c = T_0$, $L_0 = 1\,\text{m}$ and $\Delta t = 20000\tau_0$. Model I successfully completes the 3D explosion simulation, while Model II becomes unstable after $t = 0.25t_0$. This test also demonstrates that Model II is not suitable for compressible flows with shock wave. The density isosurfaces at $t = 0.125t_0$, $0.25t_0$ and $0.375t_0$ are given in figure 9. The results reported in ref. [43] are also presented for comparison. The results by the two models agree well with the results given in ref. [43] at $t = 0.125t_0$ and $0.25t_0$. Moreover, the result by Model I at $t = 0.375t_0$ is still in good agreement. Besides, the density contour by Model I at $z = 0.4$ and $t = 0.5t_0$ is also compared with result of ref. [43]. It can be found that they are in good agreement (figure 10).

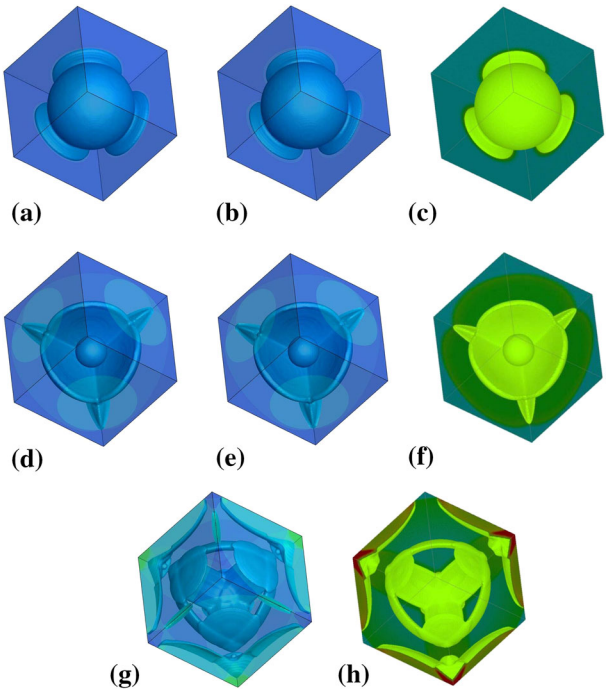

Figure 9. Density isosurfaces of 3D explosion in a box: (**a**) $t = 0.125t_0$, Model I, (**b**) $t = 0.125t_0$, Model II, (**c**) $t = 0.125t_0$, ref. [43], (**d**) $t = 0.25t_0$, Model I, (**e**) $t = 0.25t_0$, Model II, (**f**) $t = 0.25t_0$, ref. [43], (**g**) $t = 0.375t_0$, Model I, (**h**) $t = 0.375t_0$, ref. [43].

4. Conclusions

In this paper, two 3D DDF LB models for compressible flows with flexible specific-heat ratio and Pr number are developed. In the framework of coupled DDF approach, a key issue is the DVBE model. The spherical function-based D3Q25 model and Hermite expansions-based D3Q27 standard model are adopted for the 3D velocity moment condition to recover the compressible Navier–Stokes equations. Several numerical simulations of some typical compressible flows ranging from 1D to 3D are conducted to test the two 3D models. They are both capable for supersonic flows, while the latter is not suitable for compressible flows with shock wave. This work presents alternative LB models for 3D supersonic flows and shows convenience and simplicity of DDF LB approach for complex compressible flows.

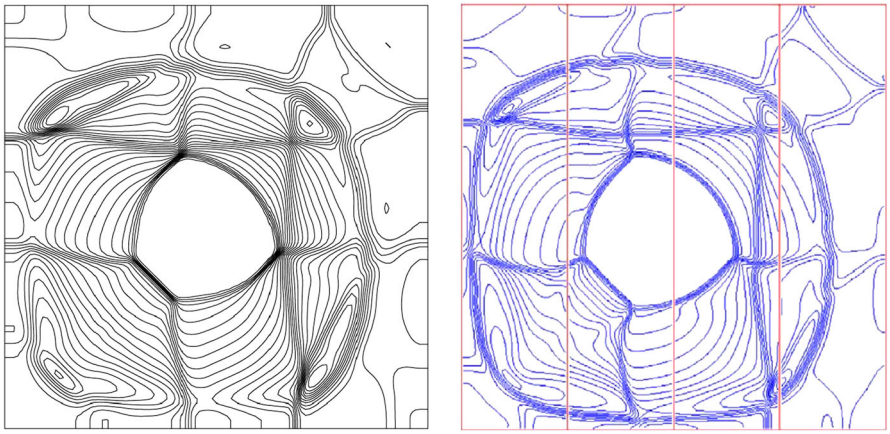

(a) **(b)**

Figure 10. Density contour of 3D explosion in a box at $z = 0.4$ and $t = 0.5t_0$: (**a**) Model I, (**b**) ref. [43].

Acknowledgements

The authors are grateful to the financial support from China Postdoctoral Science Foundation funded project under Grant No. 2016M602073, National Natural Science Foundation of China under Grant Nos 91441128, 51276151, 51606161 and 11602209, Excellent Youth Foundation of Fujian Province Natural Science Foundation under Grant No. 2016J06011, and Foundation of Fujian Province Natural Science Foundation under Grant No. 2016J01029.

References

[1] Y Qian, D D Humieres and P Lallemand, *Europhys. Lett.* **17**, 479 (1992)
[2] S Chen and G D Doolen, *Annu. Rev. Fluid Mech.* **30**, 329 (1998)
[3] S Succi, *The lattice Boltzmann equation for fluid dynamics and beyond* (Oxford University Press, New York, 2001)
[4] Y He, Q Li, Y Wang and G Tang, *Chin. Sci. Bull.* **54**, 4117 (2009)
[5] A Xu, G Zhang, Y Gan, F Chen and X Yu, *Front. Phys.* **7**, 582 (2012)
[6] S Succi, E Foti and F Higuera, *Europhys. Lett.* **10**, 433 (1989)
[7] S Chen, H Chen, D Martnez and W Matthaeus, *Phys. Rev. Lett.* **67**, 3776 (1991)
[8] Y Xu, Y Lin, X Yang and F Wu, *Commun. Theor. Phys.* **49**, 1319 (2008)
[9] T Jiang, Q Gong, R Qiu and A Wang, *Pramana – J. Phys.* **83**, 557 (2014)
[10] R Qiu, A Wang, Q Gong and T Jiang, *Int. J. Mod. Phys. C* **25**, 1450004 (2014)
[11] R Qiu, A Wang, Q Gong and T Jiang, *Comput. Math. Appl.* **70**, 244 (2015)
[12] S Leclaire, N Pellerin, M Reggio and J Y Trpanier, *Appl. Math. Model.* **40**, 6376 (2016)
[13] R Qiu and A Wang, *Comput. Fluids* **138**, 1 (2016)
[14] F J Alexander, S Chen and J D Sterling, *Comput. Fluids* **47**, R2249 (1993)
[15] G Yan, Y Chen and S Hu, *Phys. Rev. E* **59**, 454 (1999)
[16] T Kataoka and M Tsutahara, *Phys. Rev. E* **69**, 03570 (2004)
[17] K Qu, C Shu and Y T Chew, *Phys. Rev. E* **75**, 036706 (2007)
[18] M Watari, *Physica A* **382**, 502 (2007)
[19] Y Gan, A Xu, G Zhang and Y Yang, *Europhys. Lett.* **103**, 24003 (2013)
[20] A Xu, C Lin, G Zhang and Y Li, *Phys. Rev. E* **91**, 043306 (2015)
[21] X He, S Chen and G D Doolen, *J. Comput. Phys.* **146**, 282 (1998)
[22] Z Guo, C Zheng, B Shi and T S Zhao, *Phys. Rev. E* **75**, 036704 (2007)
[23] Q Li, Y He, Y Wang and W Tao, *Phys. Rev. E* **76**, 056705 (2007)
[24] Y Wang, Y He, Q Li, G Tang and W Tao, *Int. J. Mod. Phys. C* **21**, 383 (2010)
[25] Q Li, K Luo, Y He, Y Gao and W Tao, *Phys. Rev. E* **85**, 016710 (2012)
[26] Y Gan, A Xu, G Zhang, P Zhang, L Zhang and Y Li, *Commun. Theor. Phys.* **50**, 201 (2008)
[27] Y Gan, A Xu, G Zhang and Y Li, *Commun. Theor. Phys.* **56**, 490 (2011)
[28] F Chen, A Xu, G Zhang, Y Gan, T Cheng and Y Li, *Commun. Theor. Phys.* **52**, 681 (2009)
[29] F Chen, A Xu, G Zhang and Y Li, *Phys. Lett. A* **375**, 2129 (2011)
[30] T Kataoka and M Tsutahara, *Phys. Rev. E* **69**, 056702 (2004)
[31] F Chen, A Xu, G Zhang and Y Li, *Commun. Theor. Phys.* **54**, 1121 (2010)
[32] M Watari and M Tsutahara, *Physica A* **364**, 129 (2006)
[33] Q Li, Y He, Y Wang and G Tang, *Phys. Lett. A* **373**, 2101 (2009)
[34] Y He, Q Liu and Q Li, *Physica A* **392**, 4884 (2013)
[35] X He and L Luo, *Phys. Rev. E* **55**, R6333 (1997)

[36] X Shan, X Yuan and H Chen, *J. Fluid Mech*. **550**, 413 (2006)
[37] C Sun, *Phys. Rev. E* **58**, 7283 (1998)
[38] Y Feng, P Sagaut and W Tao, *Comput. Fluids* **131**, 45 (2016)
[39] S Pieraccini and G Puppo, *J. Sci. Comput.* **32**, 1 (2007)
[40] Y Wang, Y He, T Zhao, G Tang and W Tao, *Int. J. Mod. Phys. C* **18**, 1961 (2007)
[41] H Zhang, *Acta Aerodynam. Sinica* **6**, 143 (1988)
[42] Z Guo, C Zhang and B Shi, *Chin. Phys. B* **11**, 366 (2002)
[43] http://amroc.sourceforge.net/examples/euler/3d/html/box3d_c.htm